Applied Catalysis B: Environmental 325 (2023) 122289

Contents lists available at ScienceDirect

Applied Catalysis B: Environmental

journal homepage: www.elsevier.com/locate/apcatb

Photocatalytic property of WO_3 modified with noble metal co-catalysts towards selective hydroxylation of benzene to phenol under visible light irradiation

Shinya Higashimoto [a,*], Yuya Kurikawa [a], Yuki Tanabe [a], Takashi Fukushima [a], Ai Harada [a], Michihisa Murata [a], Yoshihisa Sakata [b], Hisayoshi Kobayashi [c]

[a] Department of Applied Chemistry, Faculty of Engineering, Osaka Institute of Technology, 5-16-1 Omiya, Asahi-ku, Osaka 535-8585, Japan
[b] Graduate School of Science and Technology for Innovation, Yamaguchi University, 2-16-1 Tokiwadai, Ube 755-8611, Japan
[c] Emeritus professor of Kyoto Institute of Technology, Matsugasaki, Sakyo-ku, Kyoto 606-8585, Japan

ARTICLE INFO

Keywords:
Pd/Pt-WO_3 photocatalyst
Visible light
One step hydroxylation of benzene
Selective photocatalytic reaction
Oxygen reduction reaction (ORR)

ABSTRACT

Direct synthesis of phenol from benzene in the presence of water and oxygen were conducted under visible-light irradiation. Effects of several noble metal co-catalyst on the selective hydroxylation of benzene over WO_3 photocatalysts have been extensively studied. The photocatalytic activities of WO_3 for phenol formation strongly depend on co-catalyst such as Pt, Au, Pd metal species, i.e., phenol formation was as follows: Pt-WO_3 > Au-WO_3 > Pd-WO_3. Furthermore, the WO_3 photocatalyst deposited bimetal co-catalysts such as Pd/Pt, Pd/Au and Pt/Au were also investigated. The Pd/Pt-WO_3 photocatalyst was found to show the highest photocatalytic activity for phenol formation due to an effective oxygen reduction reaction (ORR) for bimetallic Pd/Pt cocatalyst. From the experimental and theoretical studies, phenol was confirmed to form by the insertion of OH derived from H_2O into benzene, and simultaneous cleavage of benzylic carbon-hydrogen bond (C_{sp2}-H) by an assist of co-catalyst surface through the push-pull process.

1. Introduction

Phenols are important substances for industrial products such as dyes, polymers. They are practically produced by multi-step cumene process, working under high temperature, high pressure and strong acidic conditions. On the other hand, the direct hydroxylation of benzene to phenol using water as an environmentally friendly electron donor sources have attracted much attention not only over homogeneous [1–4] but also heterogeneous photocatalyst [5–11]. Therefore, it is highly desired to develop a one-step synthesis of phenol from benzene using photocatalysts at room temperature [1–4]. In recent study, the photocatalytic hydroxylation of benzene into phenol were extensively studied on the TiO_2 deposited co-catalysts such as single metals (Pt, Pd, Au) [5–10] or bimetal (Au-Pd) [11]. However, the photo-excited TiO_2 under UV-light irradiation reacted with H_2O and O_2 to form hydroxyl radical and superoxide anion species, respectively. These intermediate species led to deep oxidation of benzene into CO_2, causing low selectivity to phenol formation. To improve the selectivity from benzene to phenol, it is necessary to choose appropriate co-catalysts that determine the oxygen reducing ability for the oxygen reduction reaction (ORR); and semiconductors that are sensitive to visible-light irradiation.

The ORR has been paid much attention to development of metal catalyst for fuel cells as well as co-catalyst for photocatalytic reactions. The relationship between the stabilization energy for adsorption of O_2 on the co-catalyst and the ORR activity have been shown as a volcano plot [12]. The Pt metal is accepted to exhibit the most efficient ORR. For strongly adsorbed O_2 on metals, removal of such oxygen reducing species as the OH group, represents the rate-limiting step, whereas for metals with weakly adsorbed O_2, electron transfer to O_2 represents the rate-limiting step [12]. Electrochemical catalysis for the ORR on single metals (Pt, Au, Ag, Ru and Pd) as well as bimetals (Pd-Au, Pt-Pd, Ag-Pd) have been extensively studied [13–20]. Bimetal catalysts were found to exhibit higher electrocatalysis than the single metal catalysts, and, in particular, Pt-Pd co-catalyst exhibited the highest activity for the ORR [13,14,19,20].

Visible light-driven photocatalysts such as WO_3 and graphic carbon

Abbreviations: ORR, oxygen reduction reaction; DFT, density functional theory; C_3N_4, graphic carbon nitride; VOCs, volatile organic compounds.

* Corresponding author.
E-mail address: shinya.higashimoto@oit.ac.jp (S. Higashimoto).

https://doi.org/10.1016/j.apcatb.2022.122289
Received 31 October 2022; Received in revised form 7 December 2022; Accepted 11 December 2022
Available online 15 December 2022

nitride (C_3N_4) have been extensively studied to make the most use of sunlight in the regions of 400–800 nm [21–27]. One of the promising visible-light responsible photocatalyst is a WO_3 semiconductor. The WO_3 have been widely applied for the photocatalytic decomposition of volatile organic compounds (VOCs) [28–34], oxidative water splitting to form O_2 [35], and selective organic synthesis [36–41]. The WO_3 photocatalysts supporting Pt, Pd, or CuO co-catalysts have been developed to completely mineralize VOCs such as toluene and acetaldehyde in the gas phase and acetic acid in the liquid phase under visible light irradiation. The photocatalytic reactions can, thus, be promoted by supporting an appropriate co-catalyst on the WO_3 photocatalyst.

By controlling the oxidizing power and reducing power of the photocatalyst, it is possible to induce a partial oxidation reaction of organic compounds. Tomita et al. first reported that a one-step hydroxylation of benzene to phenol on the Pt-deposited WO_3 in the presence of O_2 and H_2O under photo-irradiation ($300 < \lambda < 500$ nm) [37,38]. The Pt-WO_3 photocatalyst was confirmed to show high conversion efficiency from benzene to phenol under visible-light irradiation [39]. However, to the best of our knowledge, effects of several noble metal co-catalyst on the selective hydroxylation of benzene over WO_3 photocatalysts have been little investigated except for the Pt-deposited WO_3 photocatalyst. It is still required to develop the photocatalyst with promising activities.

The purpose of this study was to construct a direct selective synthesis of phenol from benzene in a green and sustainable manner using a visible-light-responsive photocatalyst. Single metals (Pt, Au and Pd) as well as bimetals (Pd-Au, Pt-Pd, Au-Pd) supported WO_3 photocatalyst were systematically prepared by photo-electrochemical deposition methods. These photocatalysts were applied to photocatalytic hydroxylation of benzene in the presence of H_2O and O_2 under visible-light irradiation. The photocatalytic activities as well as reaction mechanisms were studied. In particular, the effect of the ORR of Pd-Pt bimetals on the photocatalytic activities were paid attention.

2. Experimental

2.1. Preparation of noble metals (Pt, Pd and Au)-deposited WO_3 photocatalyst

The Pt and/or Pd-deposited WO_3 (Pt-WO_3, Pd-WO_3, Pd/Pt-WO_3) photocatalyst were prepared by photo-deposition methods. Material information was provided in the experimental section of supporting information. The photo-deposition was carried out by two steps: 1) photoadsorption of metal ions on the WO_3, and 2) photoreduction into metallic species in the presence of ethanol. The Pt-WO_3 photocatalyst was prepared by photo-deposition of Pt species on the WO_3 under visible-light irradiation. The WO_3 powder (1.0 g) was suspended in distilled water (25 mL) involving desired amounts of 19.0 mM H_2PtCl_6 aqueous solution. The suspension was photo-irradiated from LED lamp ($420 < \lambda < 540$ nm, 25,000 Lux) for 2 h, and subsequently it was photo-irradiated after addition of ethanol (2 mL) for more 4 h. Furthermore, Pd was photo-deposited on Pt-WO_3 in distilled water involving desired amounts of 20.0 mM $PdCl_2$ aqueous solution and ethanol (2 mL). For preparation of Au-WO_3 photocatalyst, the WO_3 was suspended in distilled water (25 mL) involving desired amounts of 19.0 mM $HAuCl_4$ aqueous solution, and the pH was then adjusted to be 7.0 by 0.1 M NH_3 aq. After pH adjustment, light irradiation was carried out by the method described above.

Solid products were separated by a centrifuge (LC-200, TOMY, 4500 rpm). It was then washed with distilled water and acetonitrile, and dried under vacuum at ambient temperature. The photocatalyst was referred to be as Pt(x)-WO_3, Pd(x)-WO_3 and Au(x)-WO_3 (x: atomic %). Furthermore, three types of bimetal deposited WO_3 photocatalyst, i.e., Pd(y)/Pt(x)-WO_3, Pd(y)/Au(x)-WO_3, Pt(y)/Au(x)-WO_3 (x, y: atomic %) were prepared in the similar manner. Characterization procedures involving electrochemical methods were provided in the experimental section in supporting information.

2.2. Photocatalytic reactions

Photocatalyst (20 mg) was suspended in distilled water (5 or 10 mL) in a pyrex reaction tube (volume: 20 mL) under air capped with precision seal septum. If specific description was not given, the distilled water (10 mL) was introduced. And subsequently, 26.8 μL of benzene (300 μmol) was dropped into the distilled water, followed by stirring vigorously. The reaction cell was photo-irradiated from blue LED ($420 < \lambda < 540$ nm, 25,000 Lux). After the reaction, the catalysts were immediately separated from the suspension by filtration through a 0.20 μm membrane filter (Dismic-25JP, Advantec). The solution was, then, analyzed by HPLC (Shimadzu LC10ATVP, UV-Vis detector, column: Chemcopak, mobile phase: a mixture of acetonitrile and 1.0 % formic acid aqueous solution), and several products were identified (see Fig. SI 1). The half test reaction for water oxidation on the photocatalyst in the presence of 5 mM $AgNO_3$ aqueous solution was conducted under visible-light irradiation. Prior to the test reaction, the liquid phase was vigorously bubbled by Ar. The yields of CO_2 and O_2 were determined by GC-TCD (column: porapak Q, and MS 5 A), respectively. For identification of H_2O_2 formed by the photocatalytic reaction, titanium sulfate (100 μL) was added to 1 mL of the reaction solution, and the colorimetry from the value of absorbance at 410 nm in the UV-Vis absorption spectrum was evaluated.

To understand the reaction mechanisms over Pt-WO_3 and Pd/Pt-WO_3 photocatalyst, $H_2^{18}O$ was used as the oxygen isotope source in tracer experiment. Hydroxylation of benzene (300 μmol) was carried in water (5 mL, 10 % $H_2^{18}O$/ 90 % $H_2^{16}O$) with and without $H_2^{16}O_2$ (150 μmol) and air under visible-light irradiation. Phenol in aqueous solutions were extracted by toluene, and the molar ratios of Ph-^{18}OH and Ph-^{16}OH were identified by LC-MS (Shimadzu LCMS-2020 spectrometer).

2.3. DFT calculation

DFT calculation was carried out by Gaussian 09 program [42] and the hybrid B3LYP functional [43] were used. We employed hexagonal shaped Pt_{10} clusters modeling the Pt(111) surface [44,45], and the number of atoms was fixed to 10. Since the optimal atomic ratio of Pd/Pt in the experiment was close to 3, the Pt_3Pd_7 model was employed in the calculation. The structures of Pt_{10} and Pt_3Pd_7 were shown in Fig. SI 9. For the Pt_3Pd_7 cluster, the averaged value of Pt-Pt and Pd-Pd distances was adopted, and a hexagonal shape of the basal plane was maintained. For geometry optimization, the seven atoms in the basal plane were fixed, and the upper three atoms were fully optimized as well as oxygen and hydrogen atoms. For Pt and Pd atoms, the Los Alamos effective core potentials [46] were employed along with the corresponding valence double basis sets [47]. For H and O atoms, 6–311 G(d,p) basis set was used. The structures of transition states were first calculated, and then the intrinsic reaction coordinate (IRC) analysis was carried out for both directions from reactant and product sides [48].

3. Results and discussion

3.1. Selective hydroxylation of benzene to phenol under visible light irradiation on WO_3 photocatalyst modified with noble metal co-catalysts

The photocatalytic hydroxylation of benzene in the presence of H_2O and O_2 was performed on the WO_3 photocatalyst under visible-light irradiation. It was confirmed that the hydroxylation reaction does not take place under photo-irradiation without a photocatalyst nor with a photocatalyst without irradiation, i.e., both photocatalyst and irradiation are required in combination for hydroxylation reaction to occur. By the photocatalytic hydroxylation of benzene, several kinds of products were observed (See Fig. SI 1). The bare WO_3 photocatalyst exhibited very low activity and selectivity for phenol formation under visible-light irradiation (See Table SI 1). After photocatalytic reaction, the color of suspension was slightly blue, resulting in partial reduction of WO_3, of

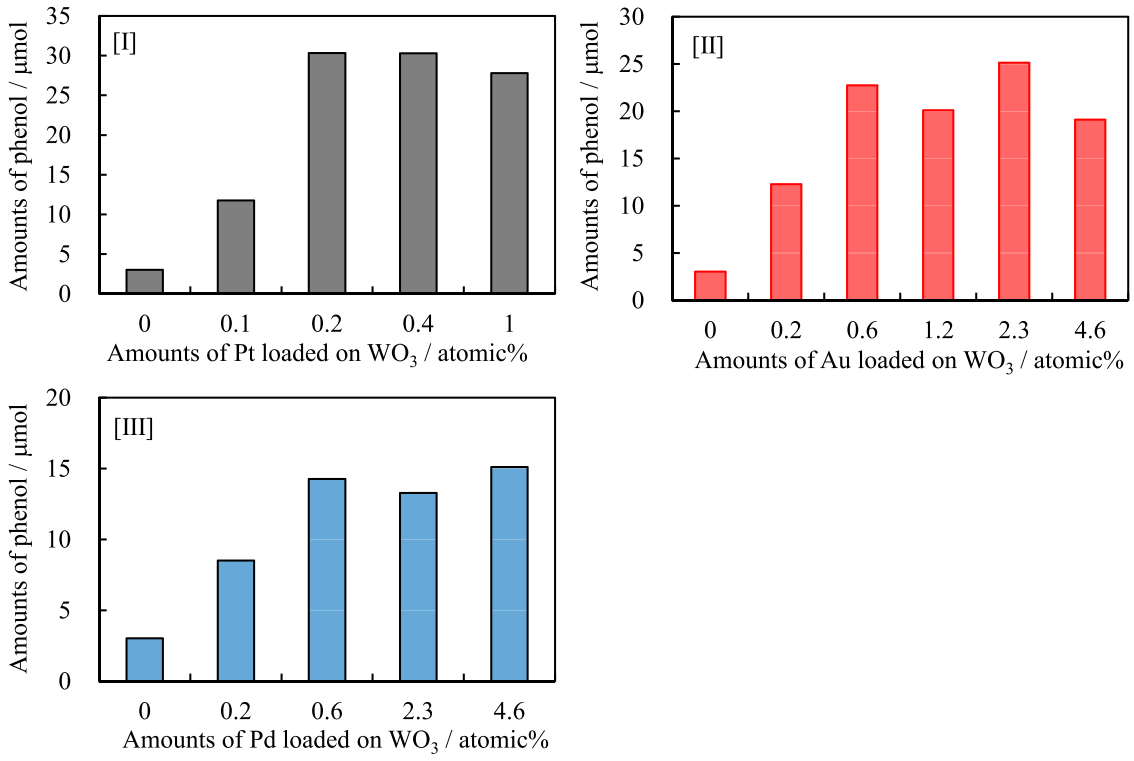

Fig. 1. Effects of loading amounts of Pt [I], Au [II] and Pd [III] deposited over WO_3 photocatalyst on the yields of phenol by photocatalytic hydroxylation of benzene.

Table 1
Photocatalytic activities for hydroxylation of benzene on Pd/Pt(0.2)-WO_3 photocatalyst with different loading amounts of Pd.

Photocatalyst	Products / μmol							Selectivity of
	PH	BQ	CA	RE	HQ	PG	PL	PH / %
Pt(0.2)-WO_3	29.0	0.04	14.5	1.4	0.2	0.9	7.0	54.7
Pd(0.15)Pt(0.2)-WO_3	41.1	0.03	20.7	3.1	1.0	1.3	6.0	56.1
Pd(0.3)Pt(0.2)-WO_3	47.7	0.02	21.1	0.5	1.0	1.2	7.8	60.1
Pd(0.6)Pt(0.2)-WO_3[(1)]	48.5	0.03	17.6	1.0	1.0	2.6	5.5	63.6
Pd(1.2)Pt(0.2)-WO_3	46.1	0.1	12.4	1.7	1.1	1.3	6.2	66.9
Pd(2.3)Pt(0.2)-WO_3	45.3	0.1	13.5	0.3	1.0	0.9	6.2	67.3
Pd(4.6)Pt(0.2)-WO_3	40.6	0.1	13.3	1.2	0.9	0.9	5.4	65.1

Reaction time (20 h), under air. (1) the H_2O_2 formed in solution was determined to be 0.98 μmol. Visible light irradiation ($420 < \lambda < 540$ nm).
PH: phenol, CA: catechol, RE: resorcinol, HQ: hydroquinone, BQ: p-benzoquinone, PL: phloroglucinol, PG: pyrogallol

which the ability for the ORR was low.

To improve the ORR efficiency, the photocatalytic reaction was examined over WO_3 deposited with metal co-catalyst. Fig. 1 shows effects of metal co-catalyst (Pt, Pd, Au) on phenol formation as a function of loading amounts of metal was shown. The product distributions are shown in supporting information (see Table SI 1 ~SI 3). As shown in Fig. 1, the Pt-WO_3, Pd-WO_3 and Au-WO_3 were observed to exhibit higher photocatalytic activities than bare WO_3. The order of photocatalytic activity for phenol formation was as follows: Pt-WO_3 > Au-WO_3 > Pd-WO_3 > > WO_3. The selectivity of phenol formation was as follows: Pt-WO_3 > Au-WO_3 > Pd-WO_3 > > WO_3. It was considered that the activity was influenced not only by the kind of co-catalyst, the particle sizes of the metals but also their dispersibility. From these results, the Pt-WO_3 photocatalyst was noticed to exhibit the highest photocatalytic performance to hydroxylation of benzene to phenol high in both yield and selectivity.

Furthermore, to improve of the photocatalytic performance, Pt-based bimetal co-catalyst deposited WO_3 photocatalyst was investigated. Table 1 shows products distribution for photocatalytic hydroxylation of benzene to phenol as a function of loading amounts of Pd deposition on the Pd(y)/Pt(0.2)-WO_3 photocatalyst. Similar

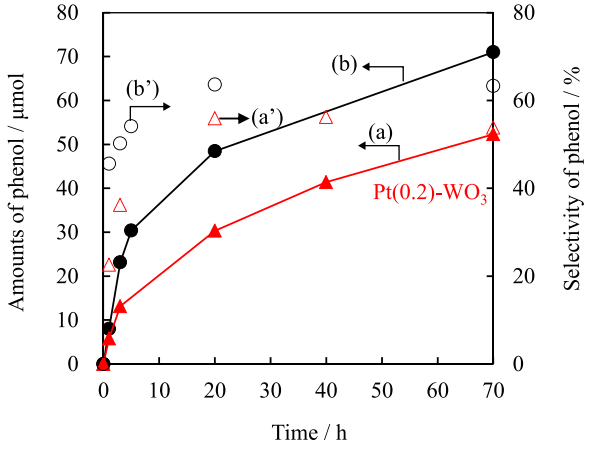

Fig. 2. Reaction time profiles on the Pt(0.2)-WO_3 (a, a′), and Pd(0.6)/Pt(0.2)-WO_3 (b, b′) for hydroxylation of benzene to form phenol (yields: a, b and selectivity: a′, b′) under visible-light irradiation.

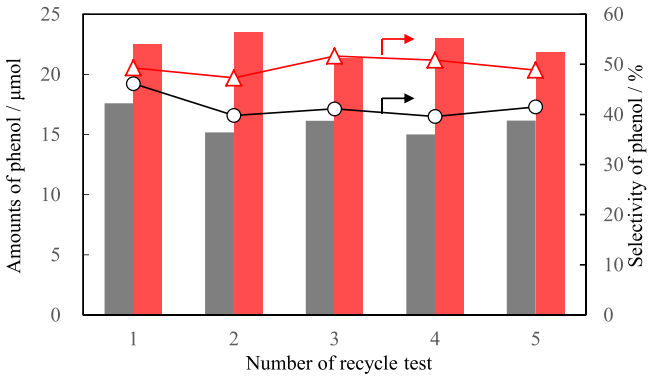

Fig. 3. Yields (gray and red bars) and selectivity (circle and triangle) of phenol photo-formed on the Pt(0.2)-WO_3 and Pd(0.6)/Pt(0.2)-WO_3, respectively. The photo-irradiation was performed for 5 h for each reaction.

examinations were conducted on Pt/Au-WO_3 and Pt/Au-WO_3 (see Table SI4 and SI5). The photocatalytic performance for hydroxylation of benzene to phenol was observed as follows: Pd/Pt-WO_3 > Pt/Au-WO_3 > > Pd/Au-WO_3. The platinum-based bimetallic cocatalysts are, thus, considered to be effective for the ORR. In the following description, the discussion was focused on the Pd/Pt-WO_3 photocatalyst exhibiting the highest activities.

It was observed that the yields and selectivity of phenol photo-formed significantly increased as an increase of amounts of Pd species, and the activity was optimized to be 0.6 at. % of Pd. Further deposition of Pd species slightly decreased the photocatalytic activities, probably due to inhibition of the light absorption of WO_3. The photocatalytic activities of Pt(0.2)/Pd(0.6)-WO_3 was higher than that of Pt(0.2)-WO_3 and Pd(0.6)-WO_3 added together, indicating that synergistic effects of bimetals were observed. Fig. 2 shows time profiles of the photocatalytic activities on Pt(0.2)-WO_3 and Pd(0.6)/Pt(0.2)-WO_3. The Pt(0.2)-WO_3 exhibited an increase of yields and selectivity of phenol with an increase of time (See Table SI 6). The Pt(0.2)-WO_3 exhibited high yields of phenol with 52.3 μmol with selectivity at 53.8 % of phenol after photo-irradiation for 70 h. On the other hand, the Pt(0.2)/Pd(0.6)-WO_3 yielded 71.0 μmol with selectivity at 63.3 % of phenol. Therefore, the Pt/Pd-WO_3 photocatalysts were confirmed to exhibit higher yields and selectivity than the Pt-WO_3. As shown in Fig. 2, the photocatalytic reaction did not proceed linearly on both photocatalyst, but activities decreased with an increase of photo-irradiation time. This is probably due to a decrease of the amount of benzene as the reactant. Fig. 3 shows recycling tests of both Pt(0.2)-WO_3 and Pd(0.6)/Pt(0.2)-WO_3 photocatalyst. The reaction was carried out by changing the reaction solution every 5 h of reaction time. These results indicated that the reaction proceeded at least 5 times without significant loss in the activity.

3.2. *Characterization of the Pd/Pt-WO_3 photocatalysts*

The Pt-WO_3, Pd-WO_3, and Pd/Pt-WO_3 photocatalysts exhibited similar XRD patterns of WO_3 with a monoclinic structure (JCPDS: 43–1035), without other phases due to Pd and/or Pt species (See Fig. SI 2). Fig. 4 shows TEM images for Pt-WO_3 and Pd/Pt-WO_3 photocatalysts. The Pt-WO_3 was observed to possess the Pt particle size (~ 5 nm), while the Pd/Pt-WO_3 possessed the Pt/Pd species (~10 nm). The EDX mapping of the Pd/Pt-WO_3 indicated that the Pd and Pt species were dispersed on the WO_3.

Fig. 5 shows XPS spectra of the Pt(0.2)-WO_3 and Pd(0.6)/Pt(0.2)-WO_3. The Pt(0.2)-WO_3 exhibited a doublet peak (4f7/2 and 4f5/2) at 71.8 and 75.2 eV due to the metallic Pt, respectively. On the other hand, Pd(0.6)/Pt(0.2)-WO_3 exhibited a doublet peak at 71.5 and 74.9 eV due to metallic Pt, and a doublet peak (4f7/2 and 4f5/2) at 335.5 and 340.7 eV due to metallic Pd. From these results, both photocatalysts were confirmed to possess mainly the metallic Pt and Pd nano species on the WO_3.

The WO_3 by itself exhibited a band-gap at ca. 450450 nmnm (2.7 (2.7 eV) due to the electronic transition of WO_3. The Pt-WO_3, Pd-WO_3 and Pd/Pt-WO_3 exhibited broad absorption above 480480 nm due to the scattering effects [49] or surface resonance [50] of the Pt and/or Pd particles (See Fig. SI 3). It was also observed that the optical absorbance above 480 nm significantly increased as an increase of loading amounts of Pt and/or Pd species. The bandgaps for the WO_3 and Pd(0.6)/Pt (0.2)-WO_3 were estimated to be ca. 2.7 eV. The Mott-Schottky plots indicated that the flatband potentials of the Pd(0.6)/Pt(0.2)-WO_3 were determined to be ca. +0.42 V vs. RHE, which is similar with that of WO_3 (+0.41 V vs. RHE). These results suggest that the flatband potentials did not significantly change by the deposition of Pt and/or Pd species (See Fig. SI 4).

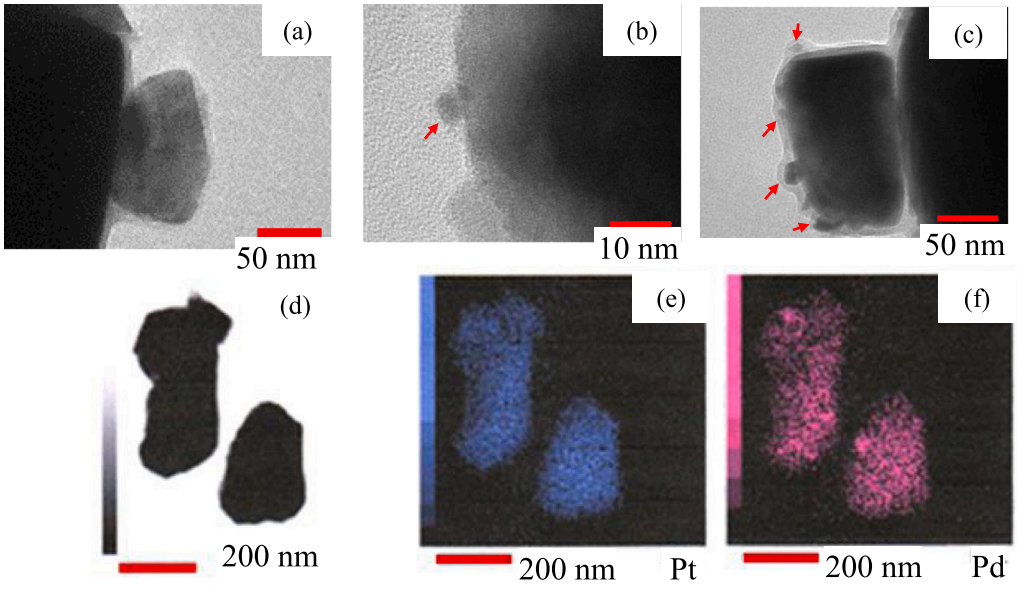

Fig. 4. TEM images of the WO_3 (a), Pt(0.2)-WO_3 (b), Pd(0.6)/Pt(0.2)-WO_3 (c, d), and EDX mappings of Pt (e) and Pd (f) elements for the Pd(0.6)/Pt(0.2)-WO_3 (d). Red arrows indicate metallic species.

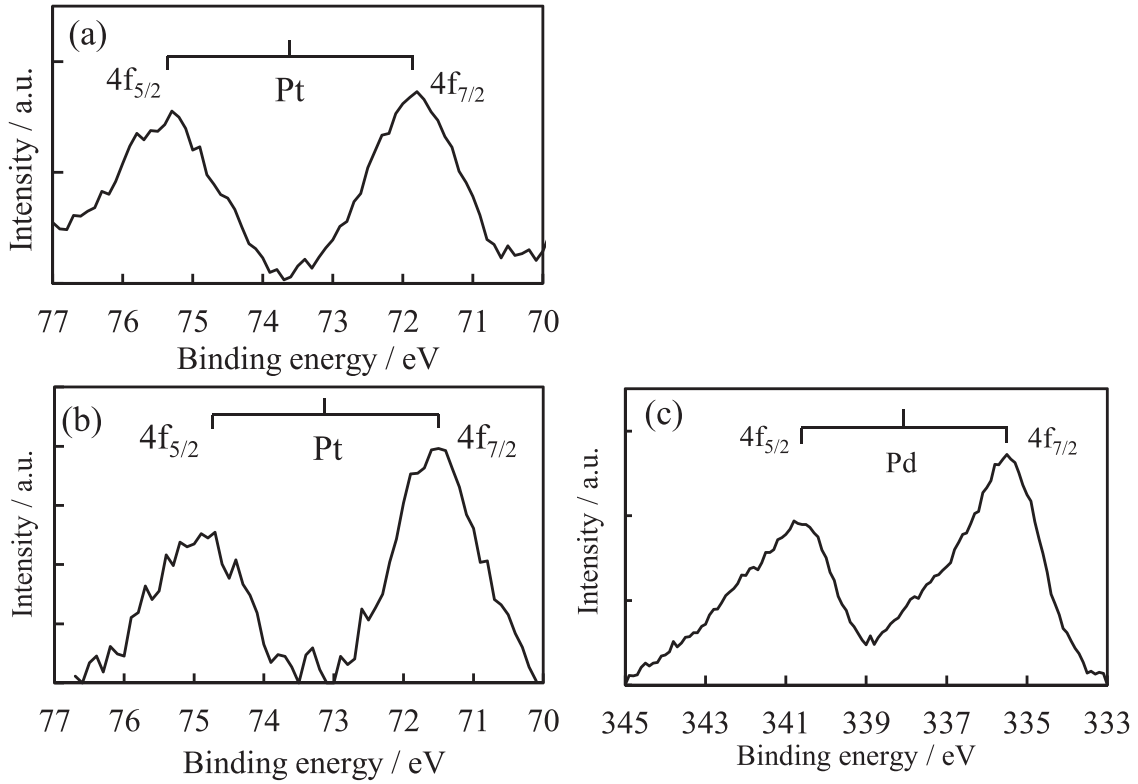

Fig. 5. XPS spectra of Pt (a, b) and Pd (c) on the Pt(0.2)-WO_3 (a) and Pd(0.6)/Pt(0.2)-WO_3 (b, c) photocatalyst.

Table 2
$H_2^{18}O$ isotope labeling test for photocatalytic hydroxylation of benzene on the Pt (0.2)-WO_3 and Pd(0.6)/Pt(0.2)-WO_3 photocatalyst.

photocatalyst	$^{18}O/^{16}O$ ratios in phenol / %	
	air [1]	air +H_2O_2 [2]
Pt(0.2)-WO_3	99	83
Pd(0.6)/ Pt(0.2)-WO_3	99	79

$H_2^{16}O$ (90 %)/ $H_2^{18}O$ (10 %) (5 mL), temperature (298 K), benzene: 300 μmol [1] visible-light for 20 h in air; [2] visible-light for 1 h, H_2O_2 (150 μmol) in air. The value shows the percentage of ^{18}OH in $H_2^{18}O$ (10 %) involved in phenol.

3.3. Role of H_2O on the photocatalytic reactions

There are two roles of water in the photocatalytic reactions. Water acts as electron donor sources: When the photocatalytic oxidation of H_2O was conducted on the Pt(0.2)-WO_3 and Pd(0.6)/Pt(0.2)-WO_3 in the presence of Ag^+ ions as electron scavenger was conducted, H_2O was oxidized by four holes to form O_2 (See Fig. SI 5). The other role of H_2O is hydroxylation of benzene. To understand role of H_2O for photocatalytic hydroxylation of benzene to phenol, the $H_2^{18}O$-labeling experiments were performed by LC-MS spectroscopy. It is noted that the atomic exchanges between O_2 and H_2O, and between O_2 and phenol are very slow even under photo-irradiation [6,51]. Therefore, $H_2^{18}O$ was used for tracing O species incorporated in phenol. The photocatalytic hydroxylation of benzene was carried out on the Pt(0.2)-WO_3 and Pd(0.6)/Pt (0.2)-WO_3 photocatalyst in H_2O (5 mL, including 90 % $H_2^{16}O$, 10 % $H_2^{18}O$) under visible-light irradiation ($\lambda > 420$ nm), and results are shown in Fig. SI 6 and Table 2. The mass number of 93 and 95 (m/z) due to the phenolic anions ($C_6H_5^{16}O^-$ and $C_6H_5^{18}O^-$), respectively, were observed. It was observed that 99 % of Ph-^{18}OH was derived from H_2O on both photocatalysts. Assuming that $H_2^{16}O$ and $H_2^{18}O$ exhibited same activity for hydroxylation of benzene, it was concluded that most hydroxyl groups derived from H_2O is substituted with benzene to form

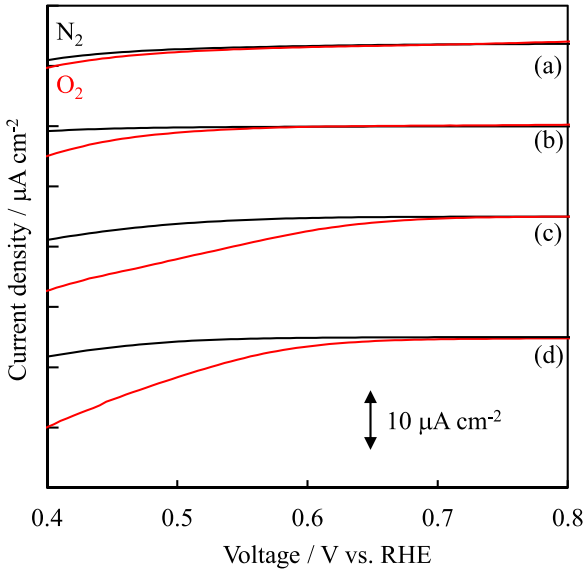

Fig. 6. Linear sweep voltammogram on WO_3 (a), Pd(0.6)-WO_3 (b), Pt(0.2)-WO_3 (c) and Pd(0.6)/Pt(0.2)-WO_3 (d) electrodes measured in 0.1 M Na_2SO_4 aq under N_2 (in black) and O_2 (in red) saturated.

phenol on the Pt(0.2)-WO_3 and Pd(0.6)/Pt(0.2)-WO_3 photocatalyst under irradiation of visible-light.

To understand rate determining step for hydroxylation of benzene on the Pt(0.2)-WO_3 and Pd(0.6)/Pt(0.2)-WO_3, the kinetic isotope effect (KIE) were determined by using D_2O and C_6D_6 (See Fig. SI 7). The KIE (k_{H2O}/k_{D2O}) on Pd(0.6)/Pt(0.2)-WO_3 were estimated to be ca. 2.6 and 1.5, respectively. On the other hand, the ratio of k_{C6H6}/k_{C6D6} for both photocatalyst was estimated to be ca. 1.0. These results suggest that the

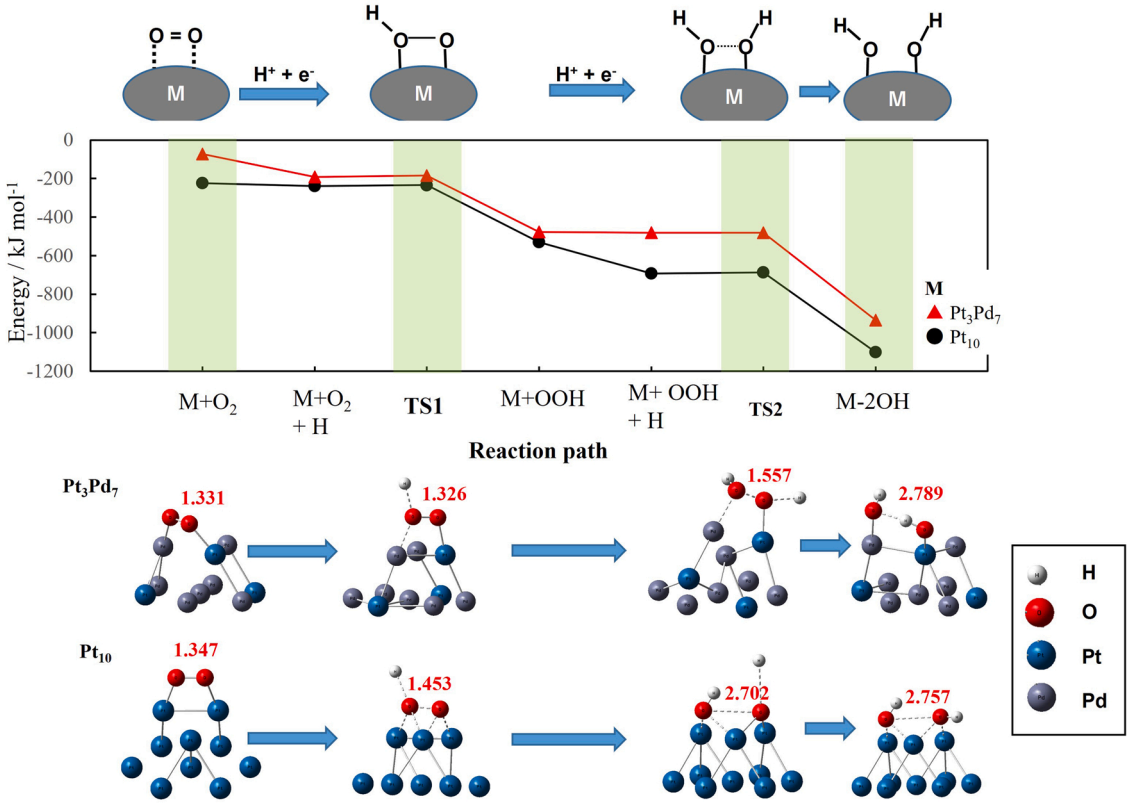

Fig. 7. Free energy profiles for ORR on metal clusters (Pt_{10} and Pt_3Pd_7) and optimized structures for reactants, TS and products. The bond length of O-O are indicated as values (Å) in red.

dissociation of O-H bond in the H_2O is the rate determining step for the hydroxylation of benzene to form phenol.

3.4. Role of O_2 on the photocatalytic reactions

To evaluate the ability for ORR of the co-catalyst, linear sweep voltammogram of WO_3 electrodes were measured in both N_2 and O_2 saturated 0.1 M Na_2SO_4 (See Fig. 6). The WO_3 was observed to exhibit little cathodic current even in the O_2 saturated solution scanned from + 0.8 to + 0.4 V vs. RHE. On the other hand, Pd and/or Pt-deposited WO_3 exhibited an increase of cathodic current in the O_2-saturated solution. Furthermore, the onset potentials of the cathodic current were estimated to be + 0.55 V for Pd(0.6)-WO_3, + 0.67 V for Pt(0.2)-WO_3 and + 0.68 V for Pd(0.6)/Pt(0.2)-WO_3. Taking the flatband potentials of WO_3 at ca. + 0.42 V vs. RHE, potentials at + 0.68 V for $E^0(O_2/H_2O_2)$ and + 1.23 V vs. RHE for (O_2/H_2O) into consideration [52], an increase of cathodic current is attributed to the ORR by multi-electrons. The efficiency of the cathodic current was as follows: Pd(0.6)/Pt(0.2)-WO_3 > Pt(0.2)-WO_3 > Pd(0.6)-WO_3. From these results, the Pd/Pt bimetal cocatalyst exhibited the ORR more effectively than either Pt or Pd cocatalyst. The efficiency of the ORR was found to correspond with the photocatalytic activity as shown in Fig. 1. Therefore, development of the ORR is very important for an improvement of the photocatalytic activity.

The photocatalytic half reactions for hydroxylation of benzene in the presence of Ag^+ ions as electron scavengers instead of O_2 were performed under visible-light irradiation. As a result, both Pt(0.2)-WO_3 and Pd(0.6)/Pt(0.2)-WO_3 exhibited little photocatalytic activities (see Table SI 7). This drastic decrease in activity is considered to be due to electron trapping in Ag^+ ions, which prevents the generation of important oxygen active species generated by ORR.

To understand the role of intermediates produced by the ORR during the reactions, the photocatalytic hydroxylation of benzene was carried out in the coexistence of H_2O_2. It is noted that the hydroxylation of benzene in the presence of H_2O_2 was not observed to take place under photoirradiation at room temperature without a photocatalyst nor with photocatalyst without irradiation. Both photocatalyst and visible-light irradiation are required for the hydroxylation of benzene. Furthermore, the photocatalytic hydroxylation of benzene was conducted in the presence of $H_2^{18}O$ and H_2O_2 instead of O_2. The percentage for ^{18}O in the phenol on Pt(0.2)-WO_3 and Pd(0.6)/Pt(0.2)-WO_3 was determined to be 83 % and 79 % of Ph-^{18}OH, respectively (See Fig. SI 6 and Table 2). These results indicate that the OH groups in phenol was confirmed to derive from H_2O mainly even in the presence of H_2O_2. In molecular photocatalysis, it was previously reported that the reducing species of O_2 was inserted as the OH group of benzene [1]. It was experimentally clarified that the OH group of water was introduced into phenol by using WO_3 photocatalyst.

3.5. DFT study on the ORR and hydroxylation of benzene

Fig. 7 shows the DFT calculation (the optimized structures and enegy diagram) for ORR process on the metal clusters (Pt_{10}, Pt_3Pd_7). The DFT calculation was carried out by using the cluster models (See Fig. SI 8), and calculation methods were mentioned in Supporting Information. It was observed that the O_2 adsorption on the Pt_{10} cluster exhibited stabilization energy larger than that on the Pt_3Pd_7 cluster. When the H atom approached on the oxygen-adsorbed metal clusters, the OOH species was formed with small activation energy (< 4.0 kJ mol^{-1}), and O-O bond distance was elongated. Then, the interactions of second H with the OOH on both metal clusters proceeded in the downhill reaction, followed by dissociation of the O-O bond to form two surface hydroxyl group.

Furthermore, Fig. 8 shows the reaction pathway for hydroxylation of benzene to form phenol on the Pt_{10} and Pt_3Pd_7 alloy catalysts. The H_2O and benzene strongly interacted with the hydroxylated metal surface. The H atom of H_2O was abstracted by surface OH, like that H_2O^* + HO-

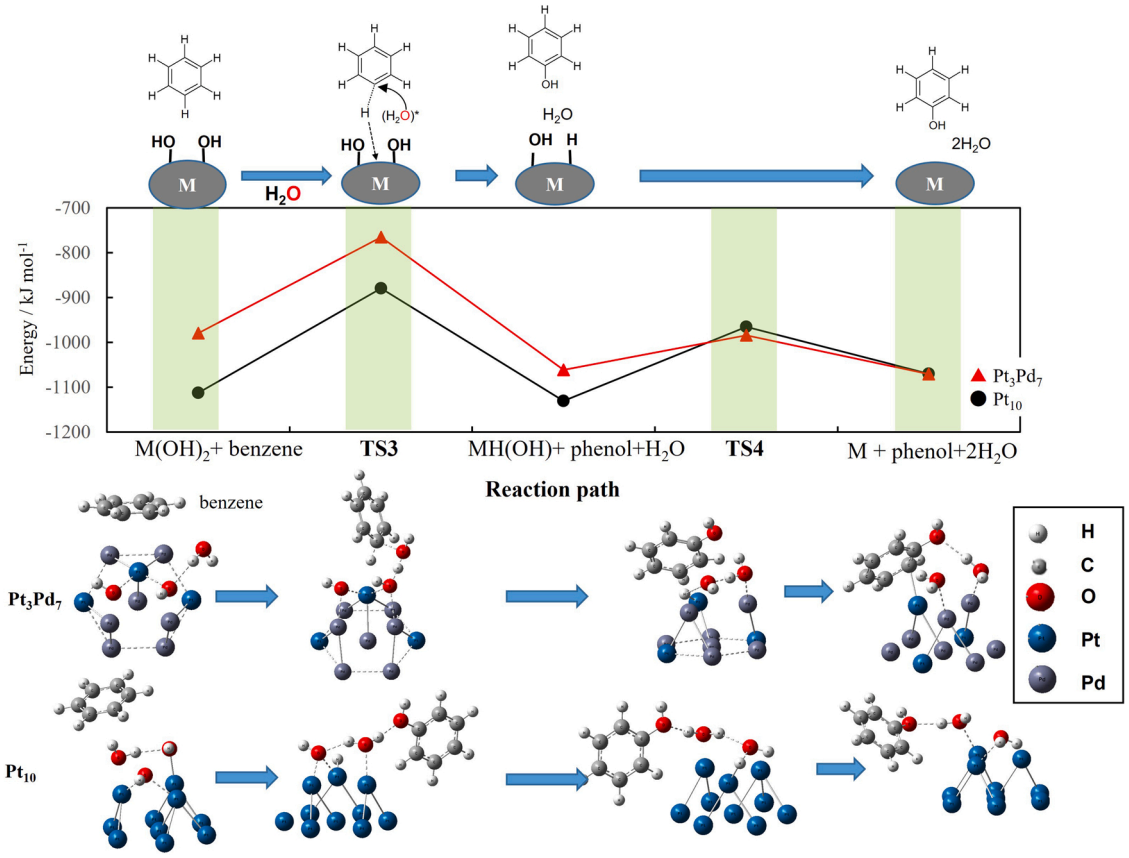

Fig. 8. Free energy profiles for hydroxylation of benzene in the presence of H_2O on partially hydroxylated metal clusters (Pt_{10} and Pt_3Pd_7), and optimized structures for reactants, TS and products.

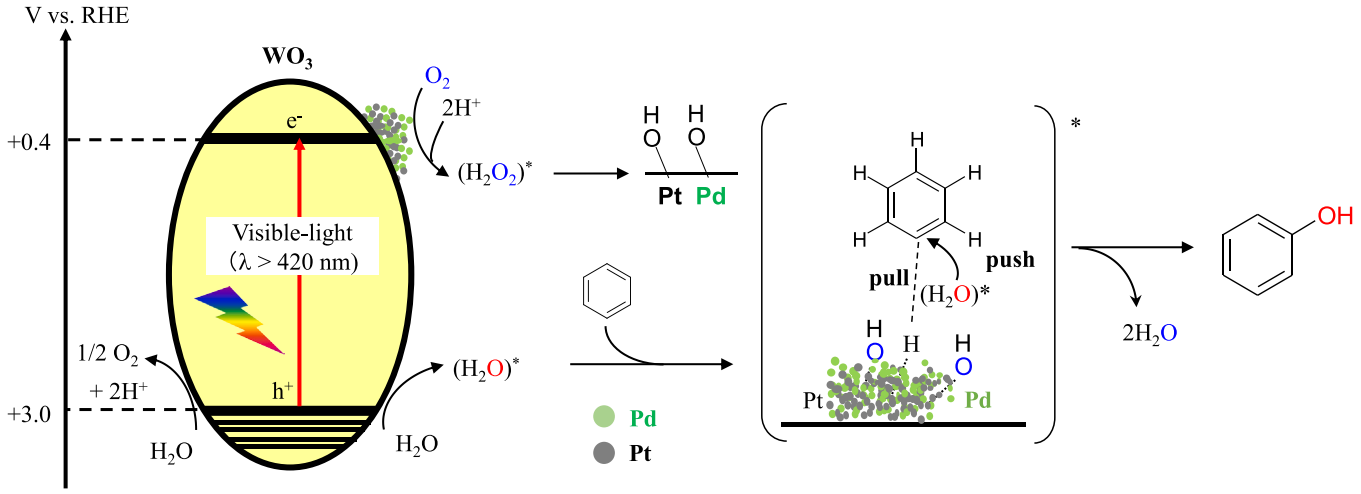

Fig. 9. Reaction mechanisms for the hydroxylation of benzene into phenol in the presence of O_2 and H_2O on the Pd/Pt-WO_3 under visible light rradiation. The $(H_2O)^*$ indicates photo-activated H_2O.

M → *OH + H_2O-M, and a newly formed *OH attacks benzene. Simultaneously the C-H bond in benzene was activated by the metal clusters to dissociate the H atom, which was embedded on the metal surface. These phenomena were, thus, in good agreement with $H_2^{18}O$ labeling experiment as mentioned above. The activation energy for water dissociation was found to be 214.2214.2 kJ mol^{-1} on the Pt_3Pd_7 lower than 233.7233.7 kJ mol^{-1} on Pt_{10}, suggesting that hydroxylation of benzene was found to occur with a lower activation energy on Pt_3Pd_7 than on Pt_{10} clusters. However, it is difficult to surpass the activation energy by a thermal reaction with more energy than 200 kJ mol^{-1}. Therefore, it could be assumed that light-energy is essentially required in the activation of water. Finally, the activation energy for liberation of OH(ad) and H(ad) on the Pt_3Pd_7 was estimated to be ca. 77 kJ mol^{-1}, which was much smaller than that on Pt_{10} (166 kJ mol^{-1}) (See Fig. 8 TS4). From these results, it is considered that the surface of Pt_3Pd_7 was seen to regenerate more easily than that of Pt_{10}. This is probably attributed to the weakened binding energy of the O* on the Pt atom influenced by Pd atoms, suggesting that Pd/Pt-WO_3 works as effective photocatalyst.

3.6. Reaction mechanism for hydroxylation of benzene to phenol on the Pd/Pt-WO_3

Fig. 9 shows the reaction mechanism for direct hydroxylation of benzene to phenol on the Pd/Pt-WO_3. Visible-light irradiation of the WO_3 induced holes and electrons in the VB and CB of the WO_3, respectively. The holes could oxidize H_2O to form O_2 and/or activated $(H_2O)^*$. On the other hand, electrons effectively transfer from the CB to O_2 via co-catalyst to form surface OH groups. By the combination of GC-MS and DFT calculations, it was confirmed that the activated $(H_2O)^*$ species would electrophilically inserted into benzylic ring to form phenol, while H moiety from benzene is attracted by metal clusters. Finally, it is considered that the reaction between the OH group and H atom embedded on the co-catalyst are liberated, resulting in generation of the intrinsic surface and catalytic cycles effectively takes place.

4. Conclusions

Environmentally friendly photocatalytic conversion of benzene to phenol was performed on WO_3-based photocatalysts in the presence of water and O_2 under visible light irradiation. The photocatalytic activity of phenol formation on WO_3 photocatalysts strongly depended on the type and amount of cocatalysts such as Pt, Au and Pd species. Photocatalytic activities of the WO_3 deposited on such bimetals as Pd/Pt and Pt/Au co-catalysts were significantly improved as compared that with the single co-catalyst. Particularly, the Pd/Pt-WO_3 photocatalyst was found to show the highest yield and selectivity for phenol formation due to high ability for the ORR. The activated H_2O was found to insert into benzylic ring to form phenol. The Pd/Pt-WO_3 photocatalysts, thus, effectively demonstrated one-step and green sustainable selective phenol formation under visible-light irradiation.

CRediT authorship contribution statement

Shinya Higashimoto: Conceptualization, Methodology, Writing-Review & Editing, Supervision, Project administration, **Yuya Kurikawa**: Methodology, Investigation, **Yuki Tanabe**: Methodology, Investigation, **Takashi Fukushima**: Methodology, Investigation, **Ai Harada**: Methodology, Investigation, **Michihisa Murata**: Writing-Review & Editing, **Yoshihisa Sakata**: Writing-Review & Editing. **Hisayoshi Kobayashi**: Methodology, Investigation.

Declaration of Competing Interest

The authors declare that they have no known competing financial interests or personal relationships that could have appeared to influence the work reported in this paper.

Data Availability

No data was used for the research described in the article.

Appendix A. Supporting information

Supplementary data associated with this article can be found in the online version at doi:10.1016/j.apcatb.2022.122289.

References

[1] K. Ohkubo, T. Kobayashi, S. Fukuzumi, Direct oxygenation of benzene to phenol using quinolinium ions as homogeneous photocatalysts, Angew. Chem. Int. Ed. 50 (2011) 8652–8655, https://doi.org/10.1002/anie.201102931.

[2] S. Fukuzumi, K. Ohkubo, One-step selective hydroxylation of benzene to phenol, Asian J. Org. Chem. 4 (2015) 836–845, https://doi.org/10.1002/ajoc.201500187.

[3] J.W. Han, J. Jung, Y.M. Lee, W. Nam, S. Fukuzumi, Photocatalytic oxidation of benzene to phenol using dioxygen as an oxygen source and water as an electron source in the presence of a cobalt catalyst, Chem. Sci. 8 (2017) 7119–7125, https://doi.org/10.1039/C7SC02495A.

[4] S. Fukuzumi, Y.M. Lee, W. Nam, Photocatalytic Oxygenation Reactions Using Water and Dioxygen 12 (2019) 3931–3940, https://doi.org/10.1002/cssc.201901276.

[5] H. Park, W. Cho, Photocatalytic conversion of benzene to phenol using modified TiO_2 and polyoxometalates, Catal. Today 101 (2005) 291–297, https://doi.org/10.1016/j.cattod.2005.03.014.

[6] T.D. Bui, A. Kimura, S. Ikeda, M. Matsumura, Determination of oxygen sources for oxidation of benzene on TiO_2 photocatalysts in aqueous solutions containing molecular oxygen, J. Am. Chem. Soc. 132 (2010) 8453–8458, https://doi.org/10.1021/ja102305e.

[7] Y. Ide, M. Matsuoka, M. Ogawa, Efficient visible-light-induced photocatalytic activity on gold-nanoparticle-supported layered titanate, J. Am. Chem. Soc. 47 (2010) 16762–16764, https://doi.org/10.1021/ja1083514.

[8] Y. Ide, M. Torii, T. Sano, Layered silicate as an excellent partner of a TiO_2 Photocatalyst For Efficient And Selective Green Fine-chemical Synthesis, J. Am. Chem. Soc. 135 (2013) 11784–11786, https://doi.org/10.1021/ja406855e.

[9] Z. Zheng, B. Huang, X. Qin, X. Zhang, Y. Dai, M.-H. Whangbo, Facile in situ synthesis of visible-light plasmonic photocatalysts M@TiO_2 (M = Au, Pt, Ag) and evaluation of their photocatalytic oxidation of benzene to phenol, J. Mater. Chem. 21 (2011) 9079–9087, https://doi.org/10.1039/C1JM10983A.

[10] T. Goto, M. Ogawa, Efficient photocatalytic oxidation of benzene to phenol by metal complex-clay/TiO_2 hybrid photocatalyst, RSC Adv. 6 (2016) 23794–23797, https://doi.org/10.1039/C5RA25430B.

[11] R. Su, L. Kesavan, M.M. Jensen, R. Tiruvalam, Q. He, N. Dimitratos, S. Wendt, M. Glasius, C.J. Kiely, G.J. Hutchings, F. Besenbacher, Selective photocatalytic oxidation of benzene for the synthesis of phenol using engineered Au-Pd alloy nanoparticles supported on titanium dioxide, Chem. Commun. 50 (2014) 12612–12614, https://doi.org/10.1039/C4CC04024D.

[12] Y. Nie, L. Li, Z. Wei, Recent advancements in Pt and Pt-free catalysts for oxygen reduction reaction, Chem. Soc. Rev. 44 (2015) 2168–2201, https://doi.org/10.1039/C4CS00484A.

[13] M. Xia, Y. Liu, Z. Wei, S. Chen, K. Xiong, L. Li, W. Ding, J. Hu, L.-J. Wan, R. Li, S. F. Alvia, Pd induced Pt(IV) reduction to form Pd@Pt/CNT core-shell catalyst for a more complete oxygen reduction, J. Mater. Chem. A 1 (2013) 14443–14448, https://doi.org/10.1039/C3TA13139D.

[14] Q. Yuan, Z.-H. Zhou, J. Zhuang, X. Wang, Pd-Pt random alloy nanocubes with tunable compositions and their enhanced electrocatalytic activities, Chem. Commun. 46 (2010) 1491–1493, https://doi.org/10.1039/B922792J.

[15] F. Gao, D.W. Goodman, Pd–Au bimetallic catalysts: understanding alloy effects from planar models and (supported) nanoparticles, Chem. Soc. Rev. 41 (2012) 8009–8020, https://doi.org/10.1039/C2CS35160A.

[16] Y. Zheng, Y. Jiao, S. Qiao, A. Vasilef, Hydrogen evolution reaction in alkaline solution: from theory, single crystal models, to practical electrocatalysts, Angew. Chem. Int. Ed. 57 (2018) 7568–7579, https://doi.org/10.1002/anie.201710556.

[17] A. Hasnat, M.M. Rahman, S.M. Borhanuddin, A. Siddiqua, N.M. Bahadur, M. R. Karim, Efficient hydrogen peroxide decomposition on bimetallic Pt–Pd surfaces, M. Catal. Commun. 12 (2010) 286–291, https://doi.org/10.1016/j.catcom.2010.10.001.

[18] Q. Jia, K. Caldwell, J.M. Ziegelbauer, A. Kongkanand, F.T. Wagner, S. Mukerjee, D. E. Ramaker, The role of OOH binding site and pt surface structure on ORR activities, J. Electrochem. Soc. 161 (2014) F1323–F1329, https://doi.org/10.1149/2.1071412jes.

[19] S. Chen, J. Zhao, H. Su, H. Li, H. Wang, Z. Hu, J. Bao, J. Zeng, Pd–Pt tesseracts for the oxygen reduction reaction, J. Am. Chem. Soc. 143 (2021) 496–503, https://doi.org/10.1021/jacs.0c12282.

[20] Zesheng Li, Bolin Li, Yifan Hu, Shaoyu Wang, Changlin Yu, Highly-dispersed and high-metal-density electrocatalysts on carbon supports for the oxygen reduction reaction: from nanoparticles to atomic-level architectures, Mater. Adv. 3 (2022) 779–809, https://doi.org/10.1039/D1MA00858G.

[21] A. Kudo, Y. Miseki, Heterogeneous photocatalyst materials for water splitting, Chem. Soc. Rev. 38 (2009) 253–278, https://doi.org/10.1039/B800489G.

[22] R. Asahi, T. Morikawa, H. Irie, T. Ohwaki, Nitrogen-doped titanium dioxide as visible-light-sensitive photocatalyst: designs, developments, and prospects, Chem. Rev. 114 (19) (2014) 9824–9852, https://doi.org/10.1021/cr5000738.

[23] J. Kou, C. Lu, J. Wang, Y. Chen, Z. Xu, R.S. Varma, Selectivity enhancement in heterogeneous photocatalytic transformations, Chem. Rev. 117 (2017) 1445–1514, https://doi.org/10.1021/acs.chemrev.6b00396.

[24] Y. Wang, H. Suzuki, J. Xie, O. Tomita, D.J. Martin, M. Higashi, D. Kong, R. Abe, J. Tang, Mimicking natural photosynthesis: solar to renewable H_2 fuel synthesis by Z-scheme water splitting systems, Chem. Rev. 118 (10) (2018) 5201–5241, https://doi.org/10.1021/acs.chemrev.7b00286.

[25] S. Higashimoto, Titanium Dioxide-based, Visible-light sensitive photocatalysis: mechanistic insight and applications, Catalysts 9 (2019) 201, https://doi.org/10.3390/catal9020201.

[26] X. Ye, Y. Cui, X. Wang, Ferrocene-modified carbon nitride for direct oxidation of benzene to phenol with visible light, ChemSusChem 7 (2014) 738–742, https://doi.org/10.1002/cssc.201301128.

[27] B. Bhuyan, M. Devi, D. Bora, S.S. Dhar, R. Newar, Design of a photoactive bimetallic Cu-Au@g-C_3N_4 catalyst for visible light driven hydroxylation of the benzene reaction through C–H activation, Eur. J. Inorg. Chem. 16 (2018) 3849–3858, https://doi.org/10.1002/ejic.201800622.

[28] J.C. Murillo-Sierra, A. Hernández-Ramírez, L. Hinojosa-Reyes, J.L. Guzmán-Mar, A review on the development of visible light-responsive WO_3-based photocatalysts for environmental applications, Chem. Eng. J. Adv. 5 (2021), 100070, https://doi.org/10.1016/j.ceja.2020.100070.

[29] R. Abe, H. Takami, N. Murakami, B. Ohtani, Pristine simple oxides as visible light driven photocatalysts: highly efficient decomposition of organic compounds over platinum-loaded tungsten oxide, J. Am. Chem. Soc. 130 (2008) 7780–7781, https://doi.org/10.1021/ja800835q.
[30] T. Arai, M. Horiguchi, M. Yanagida, T. Gunji, H. Sugihara, K. Sayama, Reaction mechanism and activity of WO_3-catalyzed photodegradation of organic substances promoted by a CuO cocatalyst, J. Phys. Chem. C 113 (2009) 6602–6609, https://doi.org/10.1021/ja800835q.
[31] T. Arai, M. Horiguchi, M. Yanagida, T. Gunji, H. Sugihara, K. Sayama, Complete oxidation of acetaldehyde and toluene over a Pd/WO_3 photocatalyst under fluorescent- or visible-light irradiation, Chem. Commun. (2008) 5565–5567, https://doi.org/10.1039/B811657A.
[32] O. Tomita, T. Sugimoto, K. Sako, S. Hayakawa, K. Katagiri, K. Inumaru, Enhanced photocatalytic activity of Pt/WO_3 photocatalyst combined with TiO_2 nanoparticles by polyelectrolyte-mediated electrostatic adsorption, Catal. Sci. Technol. 5 (2015) 1163–1168, https://doi.org/10.1039/C4CY01075B.
[33] S. Higashimoto, Y. Ushiroda, M. Azuma, Electrochemically assisted photocatalysis of hybrid WO_3/TiO_2 films: effect of the WO_3 structures on charge separation behavior, Top. Catal. 47 (2008) 148–154, https://doi.org/10.1039/C4CY01075B.
[34] S. Higashimoto, K. Katsuura, M. Yamamoto, M. Tahakashi, Photocatalytic activity for decomposition of volatile organic compound on Pt-WO_3 enhanced by simple physical mixing with TiO_2, Catal. Commun. 133 (2020), 105831, https://doi.org/10.1016/j.catcom.2019.105831.
[35] R. Abe, T. Takata, H. Sugihara, K. Domen, Photocatalytic overall water splitting under visible light by TaON and WO_3 with an IO_3^-/I^- shuttle redox mediator, Chem. Commun. (2005) 3829–3831, https://doi.org/10.1039/B505646B.
[36] O. Tomita, T. Otsubo, M. Higashi, B. Ohtani, R. Abe, Partial oxidation of alcohols on visible-light-responsive WO_3 photocatalysts loaded with palladium oxide cocatalyst, ACS Catal. 6 (2016) 1134–1144, https://doi.org/10.1021/acscatal.5b01850.
[37] O. Tomita, R. Abe, B. Ohtani, Direct synthesis of phenol from benzene over platinum-loaded tungsten (VI) oxide photocatalysts with water and molecular oxygen, Chem. Lett. 40 (2011) 1405–1407, https://doi.org/10.1246/cl.2011.1405.
[38] O. Tomita, B. Ohtani, R. Abe, Highly selective phenol production from benzene on a platinum-loaded tungsten oxide photocatalyst with water and molecular oxygen: Selective oxidation of water by holes for generating hydroxyl radical as the predominant source of the hydroxyl group, Catal. Sci. Technol. 4 (2014) 3850–3860, https://doi.org/10.1039/C4CY00445K.
[39] Y. Kurikawa, M. Togo, M. Murata, Y. Matsuda, Y. Sakata, H. Kobayashi, S. Higashimoto, Mechanistic insights into visible light-induced direct hydroxylation of benzene to phenol with air and water over Pt-modified WO_3 photocatalyst, Catalysts 10 (2020) 557, https://doi.org/10.3390/catal10050557.
[40] A. Ohno, H. Watanabe, T. Matsui, S. Somekawa, M. Tomisaki, Y. Einaga, Y. Oaki, H. Imai, Efficient photocatalytic conversion of benzene to phenol on stabilized subnanometer WO_3 quantum dots, Catal. Sci. Technol. 11 (2021) 6537–6542, https://doi.org/10.1039/D1CY01310F.
[41] W. Han, W. Xiang, J. Shi, Y. Ji, Recent advances in the heterogeneous photocatalytic hydroxylation of benzene to phenol, Molecules 27 (2022) 5457, https://doi.org/10.3390/molecules27175457.
[42] M.J. Frisch, et al., Gaussian 09, Revision D.01, Gaussian, Inc., Wallingford CT, 2013.
[43] A.D. Becke, A new mixing of Hartree–Fock and local density-functional theories, J. Chem. Phys. 98 (1993) 5648–5652, https://doi.org/10.1063/1.464304.
[44] T. Miura, H. Kobayashi, K. Domen, Density functional study of ethylene hydrogenation on Pt(111) surface, J. Phys. Chem. B 104 (2000) 6809–6814, https://doi.org/10.1021/jp993425k.
[45] Y. Shimodaira, T. Tanaka, T. Miura, A. Kudo, H. Kobayashi, Density functional theory study of anode reactions on Pt-based alloy electrodes, J. Phys. Chem. C 111 (2007) 272–279, https://doi.org/10.1021/jp064563u.
[46] P.J. Hay, W.R. Wadt, Ab initio effective core potentials for molecular calculations. Potentials for the transition metal atoms Sc to Hg, J. Chem. Phys. 82 (1985) 270–283, https://doi.org/10.1063/1.448799.
[47] T.H. Dunning Jr., P.J. Hay, in: H.F. Schaefer III (Ed.), Modern Theoretical Chemistry, vol. 3, Plenum Press, New York, 1976, pp. 1–28.
[48] K. Fukui, S. Kato, H. Fujimoto, Constituent analysis of the potential gradient along a reaction coordinate. Method and an application to methane + tritium reaction, J. Am. Chem. Soc. 97 (1975) 1–7, https://doi.org/10.1021/ja00834a001.
[49] C.W. Chen, D. Tano, M. Akashi, Synthesis of platinum colloids sterically stabilized by poly(N-vinylformamide) or poly(N-vinylalkylamide) and their stability towards salt, Colloid Polym. Sci. 277 (1999) 488–493, https://doi.org/10.1007/s003960050414.
[50] I.M. Arabatzis, T. Stergiopoulos, D. Andreeva, Characterization and photocatalytic activity of Au/TiO_2 thin films for azo-dye degradation, J. Catal. 220 (2003) 127–135, https://doi.org/10.1016/S0021-9517(03)00241-0.
[51] A.L. Buchachenko, E.O. Dubinina, Photo-oxidation of water by molecular oxygen: Isotope exchange and isotope effects, J. Phys. Chem. A 115 (2011) 3196–3200, https://doi.org/10.1021/jp111613s.
[52] M. Pourbaix, in Atlas of Electrochemical Equilibria in Aqueous Solutions, Pergamon Press Ltd, London, 1966.